Temperature tunable Bragg transmission multichannel filters made of two quarter-wave stacks separated by defect layers

IOP Publishing Eng. Res. Express 5 (2023) 015044 https://doi.org/10.1088/2631-8695/acbfa2

Engineering Research Express

CrossMark

RECEIVED
20 May 2022

REVISED
28 December 2022

ACCEPTED FOR PUBLICATION
27 February 2023

PUBLISHED
9 March 2023

PAPER

Temperature tunable Bragg transmission multichannel filters made of two quarter-wave stacks separated by defect layers

V S Bhagavan Netheti[1,2,*], B Santosh Kumar[3], M M Sandeep Kumar[4], A Chandrasekhar[2], P Kanaka Raju[2] and G Krishna Podagatlapalli[2,*]

[1] Dr. V S Krishna Government Degree College (A), Visakhapatnam-530013, Andhra Pradesh, India
[2] Department of Physics, GSS, GITAM Deemed to be University, Visakhapatnam-530045, Andhra Pradesh, India
[3] Galaxy lab, Medivalley, Andhrapradesh Medtech Zone (AMTZ), Visakhapatnam-530031, Andhra Pradesh, India
[4] Department of Mathematics, GIS, GITAM Deemed to be University, Visakhapatnam-530045, Andhra Pradesh, India
[*] Authors to whom any correspondence should be addressed.

E-mail: bhagavanphysics@gmail.com, gpodagat@gitam.edu and satguru sai.gk@gmail.com

Keywords: transmission filter, photonic bandgap, defect layer, quarter-wave, telecommunication, pico

Supplementary material for this article is available online

Abstract

We report on simulated temperature-tunable single-channel/multichannel transmission filters with 0.37 nm/K shift in the peak wavelength is observed in the infrared region (1300 nanometers −1650 nanometers) using a one-dimensional photonic crystal structure. A single channel can be selected in the photonic bandgap region based on the thickness of the quarter wave stacks and temperature. The transmission coefficient of the transmitted defect modes is approximately the same as that required for telecommunication. For 20000 defect layers, 4000 channels were created with full width at half maximum of 0.7 picometers at the center wavelength of ∼1550 nm and channel separation of ∼0.18 nanometer between 1500 nanometers-1600 nanometers.

1. Introduction

A grating is any regularly spaced collection of essentially identical, parallel, elongated elements. Generally, gratings operate in diffraction mode, Bragg reflection mode, or in the subwavelength regime. A diffraction grating is a reflecting or transparent optical component on which there are many fine, parallel, equally spaced grooves. Grating couplers will improve the coupling efficiency, polarization, and wavelength sensitivity. Roelken *et al* [1] have devised and demonstrated a grating made by adding a polysilicon layer to the existing waveguide. Thus, fabricated grating worked well as a coupler with a coupling efficiency of 78% at an input wavelength of 1.55 μm. Similarly, Cheng *et al* [2] have reported an extensive review on the principle of working, and difficulties in using grating couplers in photonics. There are reports on the gratings those work in subwavelength regimes with $Ge_2Sb_2\,Te_5$ cavity which acts as re-configurable bandpass optical filters [3]. The applications of subwavelength gratings in Si photonics and in high-speed communication are reviewed extensively [4, 5]. and n recent times, people have utilized bandpass filters as biosensors, with high sensitivity which have a tremendous lab on chip applications [6]. In the current study, we have investigated the performance of the Bragg Grating, The Bragg grating consists of periodic layered media (1-Dimensional photonic bandgap crystal) comprising alternate stacks of optically transparent substrates with different indices of refraction. With the advent of molecular beam epitaxy (MBE), the fabrication of thin films based on periodic layer media with well-controlled periodicities on the order of nanometers is quite possible [7].

If a plane wave with a suitable frequency impinges on a stacked medium, a Bloch wave is created in the stacked medium when the incident wave frequency is within the range of the photonic bandgap region. The Bloch wave generated in the stacked medium is an evanescent wave that cannot spread in the medium. Consequently, the amplitude of the electric field decreases exponentially in the stacked medium. During this process, the incident beam is reflected and the medium acts as an absolute reflector with high reflectance.

When a light beam normally impinges on the photonic crystal surface, the wavelengths that fall in the bandgap region of the photonic crystal are strongly reflected with a coefficient of reflection nearly equal to one. Wavelengths below or above the bandgap of the photonic crystal are partially or fully transmitted through the photonic bandgap (PBG) crystal [8–13]. The aforementioned PBG crystals exhibit resonance reflection and are often very similar to the secondary interference of x-rays by the atomic planes of the crystal. Therefore, photonic bandgap crystals are well-known as Bragg reflectors.

The most significant characteristic feature of photonic crystals is their photonic bandgap, in which the transmission of certain wavelengths is forbidden. The photonic bandgap changes with the refractive index, temperature, and angle of incidence of the beam [14, 15]. Consequently, this physical phenomenon allows us to design photonic crystal-based optical sensors to detect changes in the refractive index [16–22] and temperature [23, 24]. Recently, photonic crystals have gained the courtesy of researchers for their exclusive properties, making them suitable for use in various applications such as omnidirectional reflectors [25–30], filters [31–33], and very sensitive sensors in the field of optics [34].

These bandpass filters are designed and manufactured to operate in diverse regions of the electromagnetic spectrum by utilizing one dimensional photonic crystals (1DPhCs) have been reported in the past [35, 36]. These optical filters have applications in nanotechnology, astronomy, and optical communication. In our simulation, we have considered a simple case of a one dimensional (1D) stacked medium consisting of n-unit cells (i.e., n-pairs of quarter-wave films), which are separated by required number of defect layers and bounded by homogeneous media. This 1DPhC structure can be used to filter selected wavelengths in the telecommunications window [37–42]. The photonic Bragg gratings (PBGs) have their potential applications in optical communication, optoelectronics, and optical devices [43].

Wave propagation in periodic layered media can also be studied by employing the well-known transfer matrix methodology (TMM) inside photonic crystal [44–53]. The TMM method was employed to study the one-dimensional photonic crystals containing two transparent dielectric layers with diverse indices of refraction. The dielectric layers were organized in a quarter-wave stack with a defect (i.e., additional N quarter-wave layers) at the center of the stack. The structure acts as a Bragg transmission filter with multiple channels. By varying the number of quarter-wave layers in the defect layer, the desired number of defect modes that are useful for transmitting the required wavelengths can be introduced. The photonic bandgap in 1DPhC prohibits the transmission of wavelengths that fall in the PBG. Because of their simple structure, 1DPhCs are unsurpassed choices for manufacturing channel filters designed with certain specifications [54, 55].

The principle of operating a photonic Crystal (PC) as a temperature sensor is as follows: if the temperature of the surroundings of the PC changes, the refractive index of the PC structure also changes, which is a well-known thermo-optic effect [56]. Owing to the thermal expansion, the width of the photonic crystal layer increased as a function of the surrounding temperature of the PC structure. Because of the thermal expansion and thermo-optics effect, the transmission profile of the PC structure shifts into a new wavelength region according to a small variation in temperature. Using this feature of photonic crystals, we designed temperature-controlled single-channel and multi-channel filters. We have created channels that are more suitable for telecommunication applications. Our work describes the possibilities of Ultra dense wavelength division multiplexing Channels noise filtering. Temperature tunability is the added advantage of the designed filter, using this we can select the desired channel/wavelength. In the present work, the temperature-dependent tunability of the simulated filter is the novel part in comparison to our previous work [57]. The simulated multichannel filter will find its potential application in improving the optical signal-to-noise ratio (OSNR). As this filter can be completed eliminates the optical noises like amplified spontaneous emission (ASE) noise which are introduced in the process of optical amplification.

Earlier authors have proposed multichannel filters with photonic bandgap crystals but the numbers of channels in the photonic bandgap are very less, and non-uniform and the channels are not in the communication region. In our simulation work, we have created a photonic bandgap multichannel filter that can work in telecommunication regions i.e., 1500 nm to 1650 nm. The number of channels depends on the number of defect layers introduced in the structure, the channels are uniform throughout the communication wavelength region and this structure allows us to create any number of channels in the communication region based on the number of defect layers introduced in the structure. The simulated multichannel filter will find its potential application in improving the optical signal-to-noise ratio (OSNR). As this filter can completely eliminate optical noises like amplified spontaneous emission (ASE) noise which are introduced in the process of optical amplification by the EDFA and also the noise generated by the transmission through an optical fiber. The channels created in this filter are in the photonic bandgap region. So all the other wavelengths except the channel wavelength will be strongly rejected. In this way, this multichannel filter is more effective when compared with micro ring resonators (MRR), arrayed waveguide (AWG) filters and unbalanced Machzhender interferometers, etc.stacked structure is a Fabry–Perot

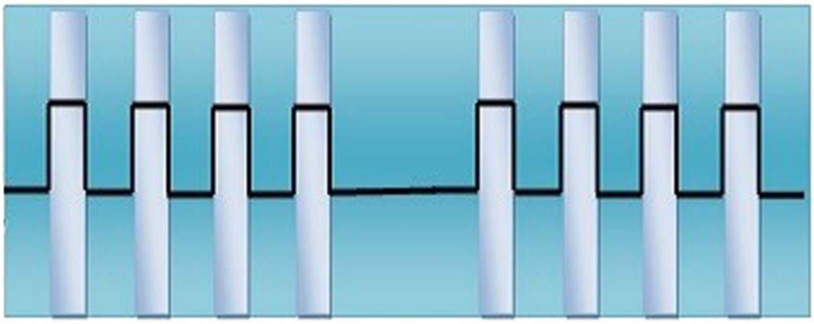

Figure 1. The physical structure of the proposed photonic crystal.

2. Data and method of analysis

In our simulation, we assumed that the materials were homogeneous, isotropic, nonmagnetic, and time reversal (nonabsorptive) in the periodic medium. The quarter-wave periodic medium comprises two dielectric transparent layers with different refractive indices, the index profile of which is shown in figure 1.

In our simulation we have used a structure like

n unit cells - N defect layers - n unit cells

Every unit cell consists of two quarter-wave films of materials with different refractive indices and periodicity is $\Lambda = a + b$. The defect layer is composed of any of the above quarter-wave layers. The transfer matrix for the structure above is expressed as follows:

$$\begin{bmatrix} a_0 \\ b_0 \end{bmatrix} = \begin{bmatrix} A & B \\ C & D \end{bmatrix}^n \begin{bmatrix} e^{ik_1 a} & 0 \\ 0 & e^{-ik_1 a} \end{bmatrix}^N \begin{bmatrix} A & B \\ C & D \end{bmatrix}^n \begin{bmatrix} a_{2n} \\ 0 \end{bmatrix} \quad (1)$$

Equation (1) relates the amplitude of the incident light wave a_0 to the amplitude of the transmitted light wave a_{2n}. The details of the above-mentioned transfer matrix method were reported in our previous work [57], and a related description is provided in the supporting information.

3. Results and discussion

In the present simulation, silica with an index of refraction $n_1 = 1.45$ was employed with a thickness $a = 269$ nm as one quarter-wave layer (P-layer) and lithium niobate with refractive index $n_2 = 2.25$ with thickness $b = 182$ nm as another quarter-wave layer (Q-layer). The defect layer in our simulation was chosen to be silica with the same thickness, as mentioned above. The structure of the layered stack is shown in figure 1.

3.1. Results and discussion

The stacked structure is a Fabry–Perot etalon with a variable cavity thickness made of silica quarter-wave layers. By inserting only one quarter-wave silica defect layer, we obtained a narrow-band transmission filter in the infrared region within the photonic bandgap of the PC structure. The transmission spectrum can be obtained by TMM [6], as described in equation (1):

Figure 2 demonstrates the transmission spectra made up of two quarter-wave stacks and their maximized versions. In generating figure 2(a), we have taken a P-layer thickness of 279 nm and a Q-layer thickness of 189 nm. The FWH of the channel at 1550.5 nm was 2.82 nm. Similarly, in plotting figure 2(c), we chose P-Layer and Q-layer thicknesses of 281 nm and 190 nm, respectively. The full width at half maximum of the channel centered at 1560.66 nm was 2.8 nm. Thus, we can obtain single transmission channels at the required wavelength by appropriately changing the thickness of quarter-wave plates.

3.2. Temperature tunable filter

We propose a structure for a temperature-tunable filter $(PQ)^7/P/(PQ)^7$ to reduce the FWHM of the defect mode to avoid inter-channel interference in dense WDM systems. The temperature tunability of the defect mode is possible because the refractive indices of silicon and lithium niobate are the pendant temperature and wavelength. In the case of silicon, the dependence of the refractive index on the wavelength and temperature obeys the following relation in the ranges 1.2 μm to14 μm and 20 °K–1600 °K [23].

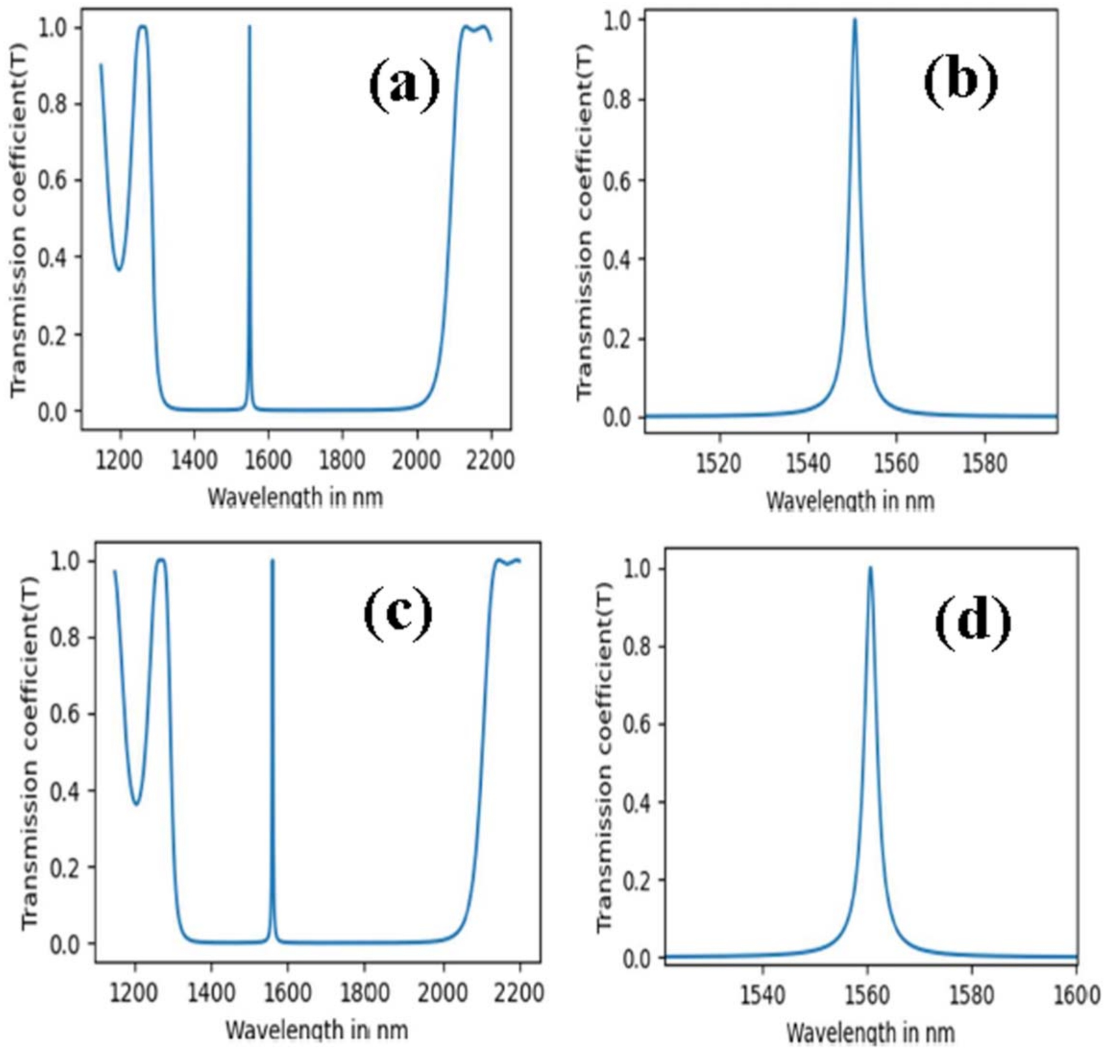

Figure 2. (a), (c) Transmission spectrum of two quarter-wave stacks with a single defect layer showing transmission channels and its magnified view (b) centered at 1550 nm and (d) at 1560 nm respectively.

$$n^2(\lambda,\ T) = \epsilon(T) + \frac{e^{-3\triangle\frac{L}{L}}}{\lambda^2}(0.8948 + 4.3977 \times 10^{-4}T + 7.3835 \times 10^{-8}T^2) \quad (2)$$

Where, $\epsilon(T) = 11.4445 + 2.7739 \times 10^{-4}T + 1.705 \times 10^{-6}T^2 - 8.1347 \times 10^{-10}T^3$
$\triangle L/L = -0.071 + 1.887 \times 10^{-6}T + 1.934 \times 10^{-9}T^2 - 4.554 \times 10^{-13}T^3$ for $293K \leqslant T \leqslant 1600K$
$\triangle L/L = -0.021 - 4.149 \times 10^{-7}T - 4.62 \times 10^{-10}T^2 + 1.482 \times 10^{-11}T^3$ for $20K \leqslant T \leqslant 293K$

In the case of lithium niobate, the refractive index varies with the wavelength and temperature according to the Sellmeier formula.

$$n^2(\lambda,\ T) = a_1 + b_1 f + \frac{a_2 + b_2 f}{\lambda^2 - (a_3 + b_3 f)^2} + \frac{a_4 + b_4 f}{\lambda^2 - {a_5}^2} - a_6\lambda^2 \quad (3)$$

The coefficient of thermal expansion for silicon is 2.6×10^{-6}/K, it is a less significant quantity. Therefore, we neglected the thermal expansion of the silicon layer in our simulations. The Sellmeier constants a_1 to a_6 are mentioned in table 1.

The thermal expansion coefficient of lithium niobate is 15.4×10^{-6}/K, which is a considerable amount. Hence, to compute the thickness of the lithium niobate layer as a function of temperature variation, the following formula was utilized:

$$t = t_0(1 + 1.54 \times 10^{-5} \times (T - 25) + 5.3 \times 10^{-9} \times (T - 25)^2) \quad (4)$$

Where t_0 is the thickness of the lithium niobate layer at 25 °C.

The proposed photonic crystal (PC) structure introduces one defect mode into the PBG. The transmission spectra of the PC with one defect at various temperatures are shown in figure 3. In this simulation, we used the thickness of silicon, that is, 273 nm for the P-layer and 185 nm for the Q-layer (lithium niobate). This structure

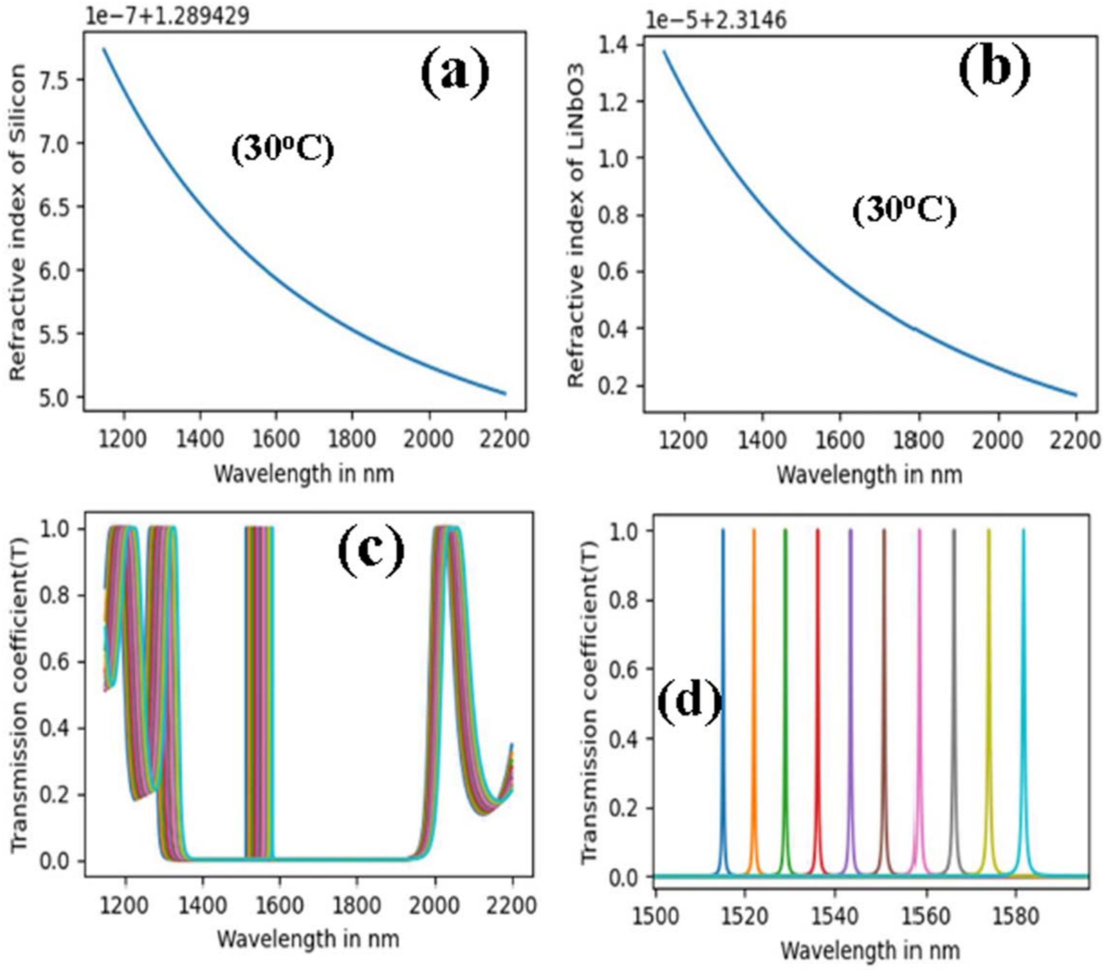

Figure 3. (a) Refractive index variation of silicon as a function of the wavelength at a constant temperature. (b) Refractive index variation of lithium niobate with respect to wavelength at a constant temperature. (c) Spectral transmission of photonic crystal structure proposed at different temperatures. (d) Zoomed version of figure (c), in this shift in central peak is clearly visible.

Table 1. The above table will give the numerical values of constants present in the Sellmeier formula.

S.no.	Constant	Value of the constant	Constant	Value of the constant
1.	a_1	5.35583	b_1	4.629×10^{-7}
2.	a_2	0.100473	b_2	3.862×10^{-8}
3.	a_3	0.20693	b_3	-0.89×10^{-8}
4.	a_4	100	b_4	2.657×10^{-5}
5.	a_5	11.34927		
6.	a_6	1.5334×10^{-2}		

exhibits a single defect mode peak at 1515.2 nm at $T = 30°$C. When the input light within a wavelength range from 1290 nm to 1960 nm incident on the proposed PC structure at $T = 30$ °C, crystal only allows the wavelength ∼1515.2 nm and the remaining wavelengths reflect from the PC. This defect mode shifts to a longer wavelength by increasing the temperature of the PC structure.

The transmission spectra (magnified) of the proposed structure at different temperatures are shown in figures 3(a)–(d) and the data are shown in table 2. From figures 3(a)–(d) and table 2, it is obvious that the central transmission peak is at 1515.2 nm at $T = 30$ °C which has been shifted to 1581.76 nm at $T = 210$ °C which indicates that the filter can be tuned over the entire telecommunication band.

As shown in table 2, as the photonic crystal temperature increases, the defect mode shifts towards the higher wavelength region. The peak position of the defect mode varies with temperature because the refractive index depends on the temperature [equations (2) and (3)]. This feature enables the design of a temperature-tunable

Table 2. The shift in central wavelength of the defect mode with respect to temperature variation.

S.No	Temperature	Peak wavelength (nm)	FWHM (nm)	Peak shift (nm)
1.	30 °C	1515.2	0.29	0
2.	50 °C	1522.06	0.3	6.86
3.	70 °C	1529.09	0.32	7.03
4.	90 °C	1536.27	0.34	7.18
5.	110 °C	1543.59	0.36	7.32
6.	130 °C	1551.03	0.38	7.44
7.	150 °C	1558.59	0.41	7.56
8.	170 °C	1566.23	0.43	7.64
9.	190 °C	1573.96	0.5	7.73
10.	210 °C	1581.76	0.52	7.8

filter in the telecommunications region. The shift in the peak wavelength of the defect mode with respect to temperature is shown in figure 3(d). It can be observed from the tabulated values that the shift in the peak wavelength is almost linear with the corresponding temperature. The average change in the peak wavelength of the defect mode is 0.3698 nm/K. This indicates that the designed photonic crystal is sensitive to temperature because the transmission channel can be tuned to the desired wavelength in a DWDM system by heating it appropriately on a temperature mount.

The FWHM of the channel slightly increases towards the higher-wavelength region, as shown in table 2. The average FWHM of the transmission channel in the telecommunication region was 0.4 nm. Today's DWDM system transmits 96 channels with 0.8 nm spacing. Consequently, this PC structure allows only a single channel through it because the average FWHM of the channel is 0.4 nm. With this designed PC structure, we have the flexibility to add or drop any DWDM channel in the telecommunications region. This PC structure suppresses optical noise and allows for signals. As a result, the optical signal-to-noise ratio (OSNR) is significantly improved. Apart from the reduction in the signal-to-noise ratio, these structures can be integrated into optical networks due to their lower thickness (~ 6.685 μm).

3.3. Temperature tunable multichannel filter

A Multichannel filter can be created by increasing the thickness of the defect layer introduced between two quarter-wave stacks. The multichannel photonic crystal structure can be expressed as $(PQ)^7/D/(PQ)^7$. Here, D is a defect layer made of silicon with a thickness of 273 nm, P-layer made of silicon with a thickness of 273 nm, and Q-layer made of lithium niobate with a thickness of 185 nm. Some of the observed peak wavelengths of the defect modes at T = 30° are 1302.84 nm, 1324.53 nm, 1347.91 nm, 1372.60 nm, 1398.48 nm, 1425.52 nm, 1483.13 nm, 1513.82 nm, 1545.82 nm, 1579.23 nm, 1614.11 nm, 1650.54 nm, 1688.60 nm, 1728.36 nm, 1728.36 nm, 1769.91 nm,1813.25 nm,1858.31 nm, 1904.69 nm, and 1951.13 nm.

The proposed photonic crystal (PC) structure introduces multiple defect modes into the PBG as shown in figure 4. The transmission spectra of the PC with multiple defect modes at different temperatures are shown in figure 4(a), figure 4(b) and their zoomed versions figures 4(c) and (d). This structure provides 20 defect modes, whose transmission peak wavelengths are given in table 3 at $T = 30$ °C. This means that the incident broadband wavelengths from 1290 nm to 1960 nm are incident on the proposed structure at $T = 30$ °C, then it will allow only 20 wavelengths listed in table 3 and the remaining wavelengths reflect from the PC structure. The entire transmission spectrum shifted towards a higher wavelength region with an increase in the temperature of the PC structure. As shown in figure 4, the defect modes shifted towards longer wavelengths as a function of the PC structure temperature.

This temperature-tunable multichannel filter provides flexibility to add or drop a certain number of channels simultaneously. By chirping the defect modes, we could tune this filter to set the desired wavelengths by increasing the temperature of the PC structure. The shifts in the peak wavelengths of the transmission channels with respect to the increase in temperature in the photonic bandgap created by the PC structure in the telecommunication region are listed in table 3. The average shift in the peak wavelength of the transmission channel is 0.517 nm/K for the proposed PC structure.

In optical communication to add/drop any channel wavelength, we employ fiber Bragg grating in combination with a circulator. But fiber Bragg grating has the limitation that it can add/drop only a single channel simultaneously. So we need to use more fiber Bragg gratings and circulators to add/drop more than one channel wavelength. But the photonic bandgap multichannel filter gives flexibility depending on the needed

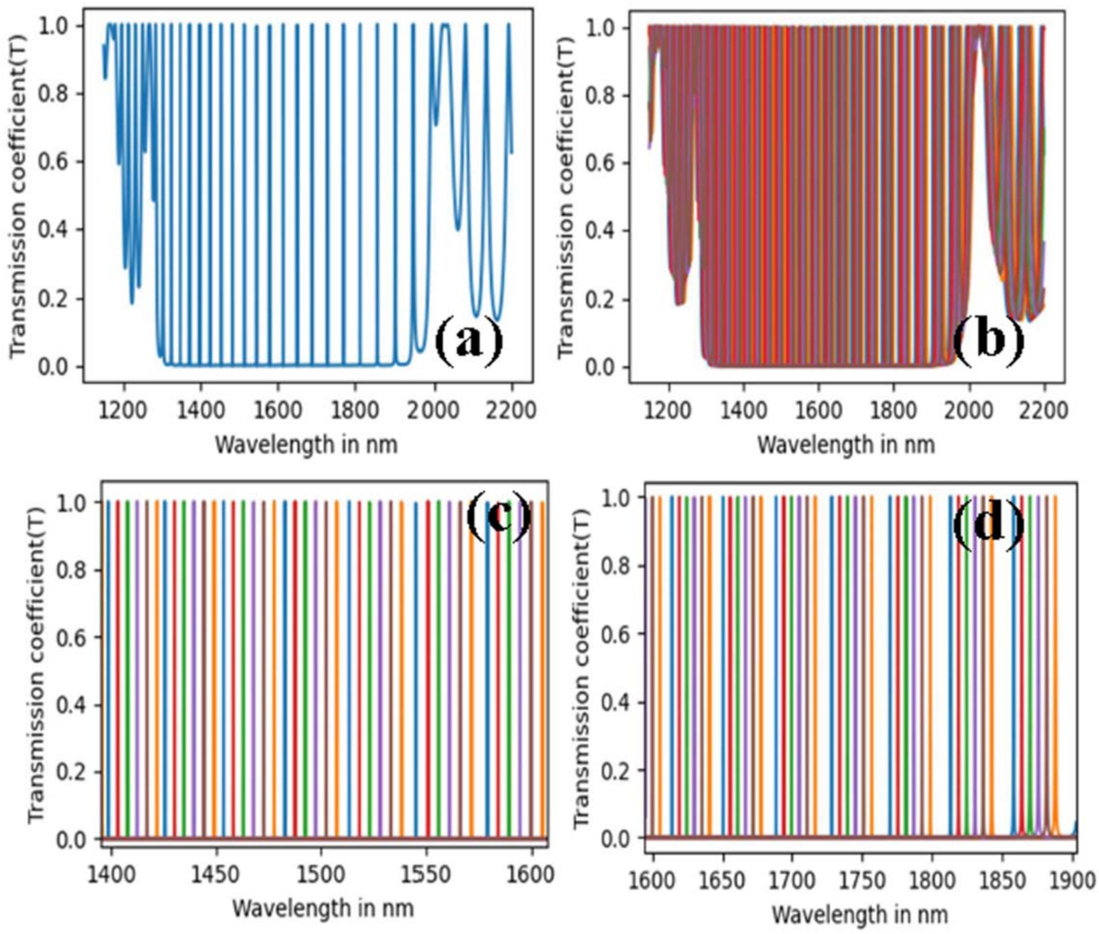

Figure 4. (a) Transmission spectrum of multichannel filter with 20 defect modes within the photonic band gap region ranging from 1290 nm to 1960 nm. (b) Transmission spectrum of temperature tunable multichannel filter within photonic band gap region at five different set of temperatures $T = 30$ °C, 40 °C, 50 °C.60 °C, 70 °C and 80 °C. (c) Zoomed version of figure (b) in the wavelength region ranging from 1400 nm to 1600 nm. (d) Zoomed version of figure (b) in the wavelength region from 1600 nm to 1900 nm.

Table 3. The shift in peak wavelengths (in nm) of transmission channels with respect to increase in temperature.

S.no.	$T = 30$ °C	$T = 40$ °C	$T = 50$ °C	$T = 60$ °C	$T = 70$ °C	$T = 80$ °C
1.	1513.82	1518.99	1524.03	1528.77	1533.81	1539.14
2.	1545.82	1551.00	1556.04	1561.08	1566.41	1571.75
3.	1579.2	1584.49	1589.53	1594.87	1600.20	1605.54

number of channels to add/drop at the nodes of the optical communication network, we can design and employ it according to the need basis. This way, a single multichannel photonic bandgap filter can replace the use of multiple fiber Bragg gratings in the network.

Temperature tunable filters are useful only when there is no availability of a multichannel filter that works in a certain band of wavelengths to add/drop the signal, and then we can tune this available multichannel filter to a required band of wavelengths by using temperature mount. But these multichannel temperature-tuneable photonic bandgap filters are not useful in dynamic operation as the required rate of switching speeds in optical communication is very high in compared with the rate of temperature tunability of the filter. We have studied in our simulation the temperature tunability of single/ multichannel filters up to high temperatures of nearly 210 °C to use as a temperature sensor. Temperature tunable single channel filters can be used as temperature sensors to monitor the temperature of rockets in space science, boilers in industries, and temperature monitoring in a hazardous environment like coal mines etc Experimental validations of the proposed multi-channel filters for real time applications is in progress.

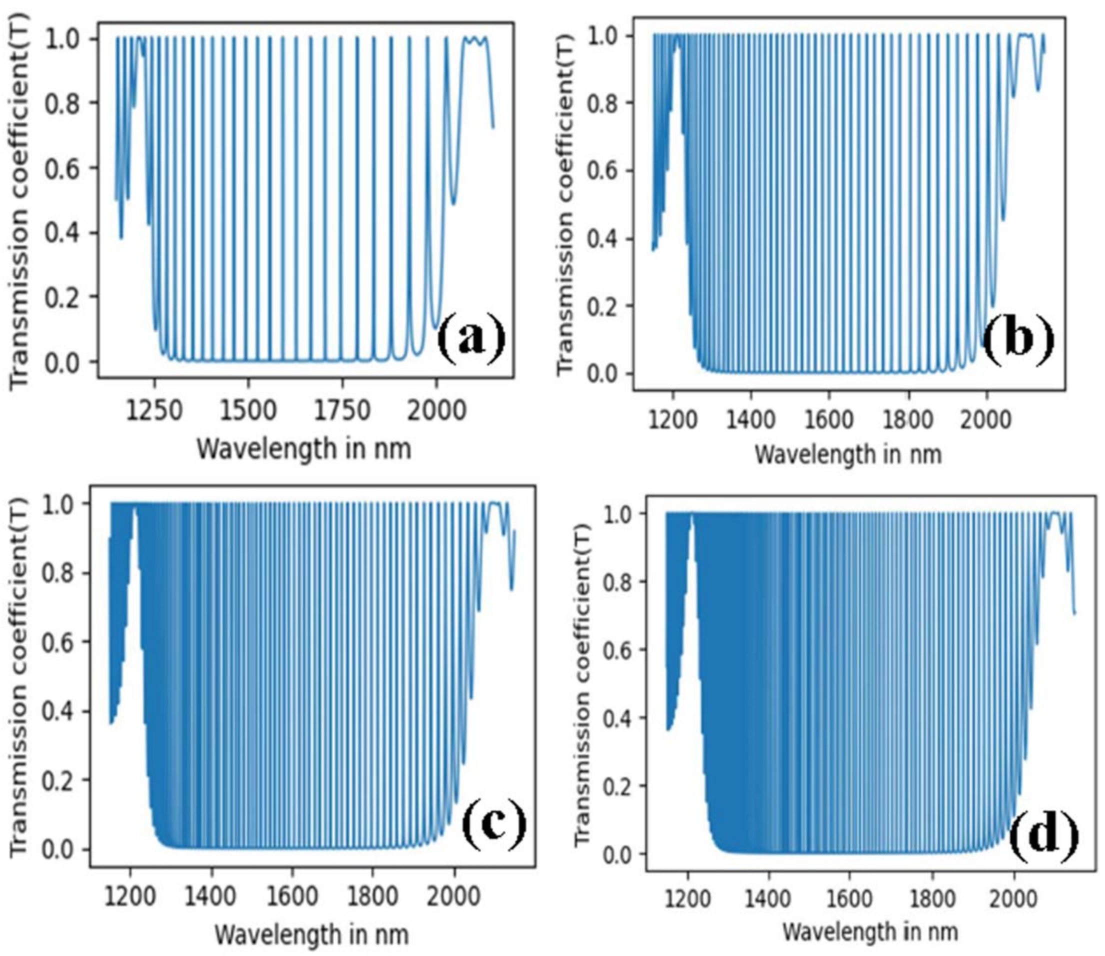

Figure 5. Transmission spectrum of a two quarter wave stacks separated by defect layer of thickness (a) D = 26.9 μm, (b) D = 53.8 μm, (c) D = 80.7 μm and (d) D = 107.6 μm respectively.

3.4. Multichannel filter for UDWDM system

Multichannel filters with different channel spacings are essential for coarse wavelength division multiplexing (CWDM) and DWDM

And UDWDM can be designed using one-dimensional photonic crystal structures. The International Telecommunication Unit (ITU-T) standardized the separation between channels to avoid inter-channel interference. The channel separation between the 16 channels in the CWDM system was 20 nm in the region of 1271 nm t0 1611 nm.

After the invention of the erbium-doped fiber amplifier, the DWDM system was developed with 40 channels with 100 GHz inter-channel spacing of 100 GHz, or 80 channels with 50 GHz inter-channel spacing in the region of 1525 nm to 1565 nm. In the UDWDM system128 channels are used for communication with 12.5 GHz inter-channel spacing, or newly developed UDWDM systems use 256 channels with 6.25 GHz inter-channel spacing. The required number of channels and interchannel spacing can be achieved by increasing the thickness of the defect layer of the proposed PC structure $(PQ)^5/D/(PQ)^5$ as shown in figure 1. In this simulation, we used silica with refractive index $n_1 = 1.45$ with thickness $a = 269$ nm as a one-quarter wave layer (P-layer), and lithium niobate with refractive index $n_2 = 2.25$ with thickness $b = 182$ nm as another quarter-wave layer (Q-layer). For the defect layer in our simulation, we chose silica material with N times the thickness of the silica quarter wave layer. We simulated the multichannel filter as a function of the thickness of the defect layer. It was observed that the number of defect modes increased with an increase in the thickness of the defect layer. The increase in the number of defect modes within the photonic bandgap region ranging from 1290 to 1960 nm for the proposed PC structure is clearly visible in the following figure 5.

Figure 5(a) consists of 20 transmission channel in the photonic band gap (PBG) region with full width at half maxima (FWHM) of channel is 0.13 nm at central wavelength 1557.57 nm and channel spacing is 33.02 nm. Figure 5(b) consists of 40 transmission channels in the PBG region with FWHM of channel is 0.06 nm at central wavelength 1549.7 nm and channel spacing is 16.83 nm. Figure 5(c) consists of 60 transmission channels in the PBG region with FWHM of channel is 0.04 nm at central wavelength 1547.02 nm and channel spacing is 11.43 nm.

Table 4. The variation of FWHM of defect modes and spacing between channels with respect to thickness of defect layer.

S.no	Number of unit cells (n)	Number of defect layers (N)	Number of modes	FWHM (nm)	Spacing between channels (nm)	Wavelengths in (~ nm) in the Infra red region
1.	10	100	20	0.13	33.02	1557.57
2.	10	200	40	0.06	16.83	1549.7
3.	10	300	60	0.04	11.43	1547.02
4.	10	400	80	0.04	8.57	1545.67
5.	10	1000	200	0.01	3.34	1550.10
6.	10	2000	400	0.006	1.72	1551.01
7.	10	3000	600	0.005	1.16	1550.16
8.	10	4000	800	0.0035	0.86	1549.74
9.	10	5000	1000	0.0027	0.7	1550.18
10.	10	10000	2000	0.0014	0.59	1550.01
11.	10	15000	3000	0.0009	0.23	1549.96
12.	10	20000	4000	0.0007	0.18	1550.11

Figure 5(d) consists of 80 transmission channels in the PBG region with FWHM of the channel is 0.04 nm at central wavelength 1545.67 nm and channel spacing is 8.57 nm. The variations of FWHM of defect modes and spacing between channels with respect to thickness of defect layer are mentioned in table 4.

The simulated multichannel filter will find its potential application in improving the optical signal-to-noise ratio (OSNR). As this filter has a potential to completely eliminate the optical noise like amplified spontaneous emission (ASE) noise which is introduced in the process of optical amplification. There is a significant improvement in the designed device (multichannel filter) when compared with previous designs whose are mention in the introductory part of the research manuscript, which is more suitable for UDWDM applications. This multichannel filter supports 600 channels between 1500 nm to 1600 nm, which is more than sufficient for required channels in telecommunication.

The proposed multi-channel filter, filter accounts for 3dB power loss at both ends. The multiplexed signal beams after getting amplified by EDFA, will emerge from the fiber out and need to be focussed by a microscopic objective lens before falling on this multilayer filter. Again, at the other end of the multilayer filter, the transmitted beam is focussed by a microscopic objective lens to launch the ASE noise-filtered light into the signal-carrying fiber. These two steps together amount to a total intensity loss of 6 dB but the noise will be completely eliminated from the multiplexed signal because these transmittance channels have been created in the photonic bandgap region. This photonic bandgap strongly rejects any kind of waves that falls in that region. In this way, this multichannel filter improves the signal-to-noise ratio significantly. Two important aspects of telecommunication are (a) Improving the signal-to-noise ratio by suppressing the noise using filters, and (b) Reducing the transmission losses of signal power. Upon employing this multichannel photonic bandgap filter after the EDFA, it effectively reduces the amplified spontaneous emission noise (ASE). The amplified spontaneous emission noise (ASE) which inherently released by EDFA. If it is not removed from the multiplexed signals, then it will be amplified because of cascading effect of optical amplification in the optical network, which results in a worsening of the signal-to-noise ratio. This designed multichannel photonic bandgap filter in our simulation is more effective in the elimination of ASE noise from EDFA as well as other noises which are generated while signal transmission through a communication network. To reduce the coupling losses of the signal power due to this filter, there is a possibility that we can inscribe this photonic crystal structure in the core of the fiber as like a Fiber Bragg grating and splicing the one end to EDFA and another end to communication fiber, which reduces power loss due to coupling dramatically. The aim of our simulation work is to create a multichannel photonic bandgap filter in the telecommunication region which is not there in previous works.

4. Conclusion

Temperature-tunable single-channel and multichannel filters were simulated. The sensitivity of the temperature tunable single channel photonic crystal filter is 0.37 nm/1°C around 1551 nm which gives the flexibility to add /drop closely spaced channels in the UDWDM system. A multi-channel filter with a 1D photonic crystal (FWHM = 0.7 pm and channel spacing (0.18 nm) were designed to suppress the amplified spontaneous emission (ASE) noise, which emanates from an inline erbium-doped fiber amplifier (EDFA). The simplicity of the proposed multichannel photonic bandgap crystal design allows easy fabrication and integration onto a photonic chip because of its minimal thickness. The special features of the multichannel filters made them flexible for use in telecommunication to improve the optical signal-to-noise ratio in the UDWDM system.

Acknowledgments

The authors acknowledge the Department of Physics, GSS, GITAM, Visakhapatnam, India, for their continuous support.

Data availability statement

The data generated and/or analyzed during the current study are not publicly available for legal/ethical reasons but are available from the corresponding author upon reasonable request.

Conflicts of interest

The authors do not have any conflicts of interest to declare.

Funding statement

There is no external funding for the proposed work.

Ethical compliance

All procedures performed in studies involving human participants were in accordance with the ethical standards of the institutional and/or national research committee and with the 1964 Helsinki Declaration and its later amendments or comparable ethical standards.

ORCID iDs

G Krishna Podagatlapalli https://orcid.org/0000-0002-3644-8734

References

[1] Roelkens 1 G, Thourhout D V and Baets R 2006 High-efficiency silicon-on-insulator grating coupler based on a poly-silicon overlay *Opt. Exp* **14** 11622–30
[2] Cheng L, Mao S, Li Z, Han Y and Fu H Y 2020 Grating couplers on silicon photonics: design principles, emerging trends and practical issues *Micro Machines* **11** 1–25
[3] Badri S H, Gilarlue M M, Farkoush S G and Rhee S B 2021 Reconfigurable bandpass optical filters based on subwavelength grating waveguides with a $Ge_2Sb_2Te_5$ cavity *J. Opt. Soc. of Am. B* **38** 1283–9
[4] Gonzalez J M L *et al* 2021 A review of silicon subwavelength gratings: building break-through devices with anisotropic metamaterials *Nanophotonics* **10** 2765–97
[5] Badri S H and Gilarlue M M Silicon nitride waveguide devices based on gradient-index lenses implemented by subwavelength silicon grating metamaterials *Appl. Opt.* **59** 5269–75
[6] Badri S H, Nahaei S S and Kim J S 2021 Hybrid plasmonic slot waveguide with a metallic grating for on-chip biosensing applications *Appl. Opt.* **60** 7828–33
[7] Herman M A and Sitter H 2012 *Molecular Beam Epitaxy: fundamentals and Current Status, Springer Series In Materials Science* 2nd edn vol 7, p 289
[8] Yablonovitch E 1987 Inhibited spontaneous in solid state physics and electronics *Phys. Rev. Lett.* **58** 2059–62
[9] John S 1987 Strong localization of photons in certain disordered dielectric superlattices *Phys. Rev. Lett.* **58** 2486–9
[10] Sakoda K 2001 *Optical Properties of Photonic Crystals* (Berlin: Springer-Verlag)
[11] Joannopoulos J D, Meade R D and Winn J N 1995 *Photonic Crystals: Molding the Flow of Light* (Princeton, NJ: Princeton University Press)
[12] Skorobogatiy M and Yang J 2009 *Fundamentals of Photonic Crystal Guiding* (Cambridge University Press)
[13] Xu B, Zheng G and Wu Y 2015 Narrow band and angle insensitive filter based on one dimensional photonic crystal containing graded index defect *Mod. Phys. Lett. B* **29** 128–36
[14] Kumar V, Suthar B, Kumar A, Singh Kh S and Bhargava A 2013 The effect of temperature and the angle of incidence on photonic band gap in a dispersive Si-based one dimensional photonic crystal *Phys. B- Condens. Matter* **416** 106–9
[15] Suthar B, Kumar V, Kumar A, Singh K S and Bhargava A 2012 Thermal expansion of photonic band gap for 1-D photonic crystals *Prog. Electromagn. Res. Lett.* **32** 81–90
[16] Shaheen A and Taya S A 2017 Propagation of p-polarized light in photonic crystal for sensor application *Chin. J. Phys.* **55** 571–82
[17] Taya S A, Shaheen S A and Alkanoo A A 2017 Photonics crystal as a refractometric sensor operated in reflection mode *Sup. Latt. Microstruct.* **101** 299–305
[18] Alkanoo A A and Taya S A 2018 Theoretical investigation of five layer wave guide structure including two left-handed material layers for refractometric applications *J. Magn. Mater* **449** 395–400
[19] Taya S A, Mahdi S S, Alkanoo A A and Qadoura I M 2017 Slab wave guide with conducting interfaces as an efficient optical sensor TE case *J. Mod. Opt.* **64** 836–43

[20] Taya S A 2015 Theoretical investigation of slab wave guide sensor using anisotropic metamaterials *Opt. Appl.* **45** 405–7
[21] Taya S A 2015 P- polarized surface waves in a slab wave guide with left-handed material for sensing applications *J. Magn. Magn. Mater.* **377** 281–5
[22] Taya S A 2014 Slab wave guide with air core layer and anisotropic left-handed material cladding as a sensor *Opto-Electron. Rev.* **22** 252–7
[23] Banerjee A 2009 Enhanced temperature sensing by using one dimensional ternary photonic band gap structures *Prog. Electromag. Res. Lett.* **11** 129–37
[24] Kai T, Wei C W, Hui Y G and Quan L Z 2007 Study on temperature property of band structures in one-dimensional photonic crystals *Optoelectron. Lett.* **3** 0444–7
[25] Awasthi S K, Malaviya U and Ojha S P 2006 Enhancement of omnidirectional total-reflection wavelength range by using one dimensional ternary photonic band gap material *J. Opt. Soc. Am. B* **23** 2566–71
[26] He J, Liu P, He Y and Hong Z 2012 Narrow bandpass tunable terahertz filter based on photonic crystal cavity *Optical Society of America* **51** 776–9
[27] Han P and Wang H Z 2003 Extension of omnidirectional reflection range in one-dimensional photonic crystals with staggered structure *J. Opt. Soc. Am. B* **20** 1996–2001
[28] Srivastava R, Thapa K B, Pati S and Ojha S P 2008 Omni-direction reflection in one dimensional photonic crystal *Prog. Electromag. Res. B* **7** 133–43
[29] Fan S, Villeneuve P R and Joannopoulos J D 1994 Large omnidirectional band gaps in metallodielectric photonic crystals *Phys. Rev. B* **54** 11245–52
[30] Malaviya S K U and Ojha S P 2006 Enhancement of omnidirectional total-reflection wavelength ranges by using one-dimensional ternary photonic bandgap material *J. Opt. Soc. Am. B* **23** 2566–71
[31] Awasthi S K and Ojha S P 2008 Design of a tunable optical filter by using one dimensional ternary photonic band gap material *Prog. Electromagn. Res. M* **4** 117–32
[32] Usievich B A, Prokhorov A M and Sychugov V A 2002 A photonic-crystal narrow-band optical filter *Las. Phys.* **12** 898–902
[33] He J, Liu P, He Y and Hong Z 2012 Narrow bandpass tunable terahertz filter based on photonic crystal cavity *Optical Society of America* **51** 776–9
[34] Banerjee A 2009 Enhanced refractometric optical sensing by using one dimensional ternary photonic crystals *Prog. Electromagn. Res. PIER* **89** 11–22
[35] Ganesh N and Cunningham B T 2012 *Appl. Phys. Lett.* **88** 071110
[36] Gryga M, Ciprian D, Gembalova L and Hubina P 2023 *Crystals* **13** 93
[37] Wu C J, Lee Y J, King T C and Kuo W K 2013 A multichannel filter based on the finite plasma photonic crystal *Key. Eng. Mat.* **538** 297–300
[38] Chang T W and Wang C J 2013 Analysis in a photonic crystal multichannel filter containing coupled defects *Optik* **124** 2028–32
[39] Awasthi S K and Ojha S P 2008 Design of a tunable optical filter by using a one dimensional ternary photonic ban gap material *Prog. In Electromag. Res* **4** 117–32
[40] Gharaati A and Azarshab H 2012 Characterization of defect modes in one-dimensional ternary metallo-dielectric nanolayered photonic crystal *Prog. In Electromag.Res. B* **37** 125–41
[41] Gharaati A and Azarshab H 2011 Characterization of defect modes in one dimensional binary metallo-dielectric nanolayered photonic crystal *Int. J. Phys* **4** 149–62
[42] Azarshab H and Gharaati A 2017 Analysis of tuning channel filter based on ternary lossy defective metallo-dielectric nano photonic crystal *Prog. Electromag. Res. Lett.* **68** 113–9
[43] Khodadadi R 2012 Adjustable filters for optical communications systems based on one-dimensional photonic crystal structures *Int. J. Eng. Res. Appl. (IJERA)* **2** 272–6
[44] Yeh P 2005 *Optical Waves in Layered Media* (New York: Wiley)
[45] Tang K, Xiang Y and Wen S 2005 Tunable transmission and defect mode in one-dimensional ternary left-handed photonic crystal *Proc. of SPIE, 60200S.1–60200S*
[46] Topasna D M and Topasna G A 2009 Numerical modeling of thin film optical filters *Education and Training in Optics and Photonics (ETOP)* 230–9
[47] Jackson J D 1999 *Classical Electrodynamics* (California University) 3rd edn vol 311
[48] Skorobogatiy M and Yang J 2009 *Fundamentals of Photonic Crystal Guiding* (Cambridge University Press) vol 132
[49] Markos P and Soukoulis C M 2008 *Wave Propagation: From Electrons To Photonic Crystals And Left Handed Materials* (New Jersey: Princeton University Press)
[50] Wu C J, Chung Y H and Syu B J 2010 Band gap extension in a one-dimensional ternary metal dielectric photonic crystal,' Prog. Electromagnet *Res* **102** 81–93
[51] Born M and Wolf E 1999 Principles of Optics, Cambridge London
[52] Saaleh B E A and Teich M C 2007 *Fundamentals of Photonics* (New York: Wiley)
[53] Loschialpo M J P and Schelleng J 2000 Photonic band gap structure and transmissivity of frequency dependant metallic-dielectric systems *J. Appl. Phys.* **88** 5785–90
[54] Kumar R, Sharma S, Singh K S, Kumar V and Jain D 2013 Design of a transmission TM mode filter using one-dimensional ternary photonic crystal *Proc. AIP Conference Proceeding* (AIP Publishing)
[55] Aming A and Chitaree R 2015 *Design of Channel Filter based on Asymmetric One-Dimensional Defective Photonic Crystal for Broadband Responses Proceedings of the International Multi-Conference of Engineers and Computer Scientists 2015 Vol II, IMECS 2015, March 18 - 20, Hong Kong*
[56] Li H H 1980 Refractive index of silicon and germanium and its wavelength and temperature derivatives *J. Phys. Chem.* **9** 561–658
[57] Bhagavan V S *et al* 2021 Multi-channel filter for UDWDM system designed based on stacking of Fabry–Perot etalons *Opt. Commun.* **4** 2630–41